Vol 16 No 1, January 2007
1009-1963/2007/16(01)/0200-07

Chinese Physics

© 2007 Chin. Phys. Soc.
and IOP Publishing Ltd

The first results of divertor discharge and supersonic molecular beam injection on the HL-2A tokamak*

Yao Liang-Hua(姚良骅)†, Yuan Bau-Shan(袁保山), Feng Bei-Bin(冯北滨), Chen Cheng-Yuan(陈程远), Hong Wen-Yu(洪文玉), and Li Ying-Liang(李英量)

Southwestern Institute of Physics, Chengdu 610041, *China*

(Received 6 December 2005; revised manuscript received 8 March 2006)

HL-2A tokamak is the first tokamak with divertors in China. The plasma boundary and the position of the striking point on the target plates of the HL-2A closed divertor were simulated by the current filament code and they were in agreement with the diagnostic results in the divertor. Supersonic molecular beam injection (SMBI) system was first installed and tested on the HL-2A tokamak in 2004. In the present experiment low pressure SMBI fuelling on the HL-2A closed divertor was carried out. The experimental results indicate that the divertor was operated in the 'linear regime' and during the period of SMB pulse injection into the HL-2A plasma the power density convected at the target plate surfaces was 0.4 times of that before or after the beam injection. It is a useful fuelling method for decreasing the heat load on the neutralizer plates of the divertor.

Keywords: supersonic molecular beam injection (SMBI), HL-2A tokamak, closed divertor, simulation

PACC: 5265, 5255, 5255G, 4755C

1. Introduction

HL-2A tokamak is the first tokamak with divertors in China.[1] The main parameters of the machine are $R = 1.65\,\mathrm{m}$, $a = 0.4\,\mathrm{m}$, $B_t = 2.8\,\mathrm{T}$ and $I_p = 0.48\,\mathrm{MA}$. The divertor of HL-2A is characterized with two closed divertor chambers, but now it is operating with lower single null configuration. The objectives of divertor design are:[2] (1) the wide dispersal of plasma power exhausted from the main plasma; (2) the production of sufficiently high gas pressures in the vicinity of pump ducts to enable the removal of fuel and helium (α particles) gas from the system; (3) the elimination or reduction of impurity production; (4) the screening of impurities produced at the plasma boundary from the plasma core. Normally, the separatrix is an interface between main plasma and scrape-off-layer (SOL). The plasma particles within the SOL, including the impurity particles created from plasma-wall interaction, may be introduced along the magnetic lines into the divertor and strike on the neutralized plates, and the resulted neutral gas can be exhausted by the pumping system.

The plasma shape and position of the plasma column can be determined from external magnetic measurements in HL-2A. The current filament (CF) model was adopted to quickly identify the plasma boundary and the magnetic surface outside the last closed flux surface (LCFS) of the single null divertor.[3]

Supersonic molecular beam injection (SMBI) system[4−6] with LN_2 cooling trap was first installed and tested on the HL-2A tokamak in 2004. The primary experiments of low pressure SMBI on the HL-2A plasma were carried out. During SMBI, the variation of the power density convected at the target plate surface was significantly reduced in comparison with that before or after the beam injection.

2. Experimental set-up of SMBI system in HL-2A

The experimental set-up of SMBI system in HL-2A and the detail structure of the molecular beam valve with cooling trap are shown in Fig.1. The valve used for producing supersonic molecular beam is a solenoid valve S99 with a Laval nozzle orifice of 0.2 mm diameter. The distance between the nozzle of the valve and the edge plasma is about 1.28 m, which is three times longer than the distance for the SMBI in

*Project supported by the National Science Foundation of China (Grant Nos 19775011, 10075016 and 10475024).
†Corresponding author. E-mail: yaolh@swip.ac.cn

the HL-1M tokamak.[6] To maintain a low background pressure during the beam injection, a turbo-molecular pump with pumping capacity $450\,\mathrm{L{\cdot}s^{-1}}$ is installed in the injection tube. A 5 mm thick of tempered steel barrel is applied for shielding the valve against stray magnetic field from HL-2A magnetic system.

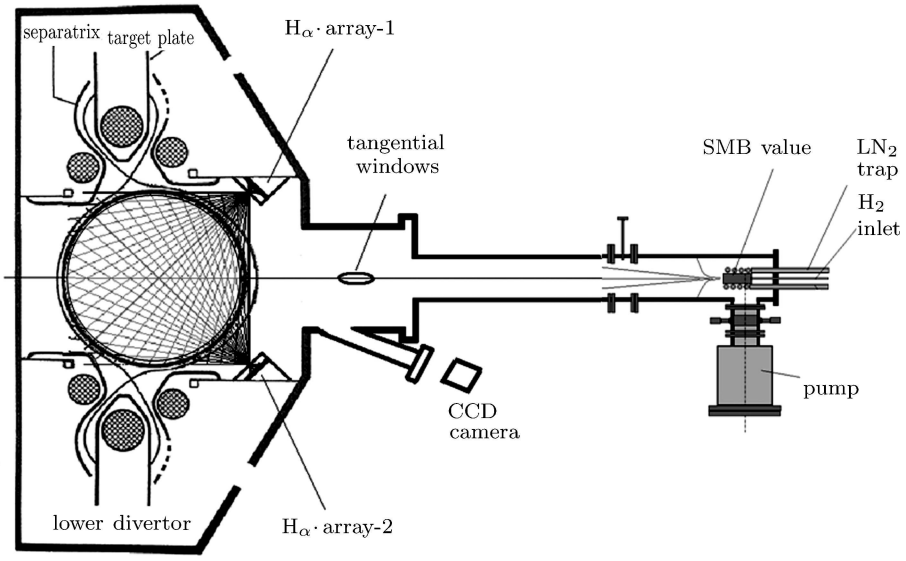


Fig.1. Supersonic molecular beam injection system in the HL-2A tokamak.

H_α signals from the edge plasma were used to observe the variation of electron temperature and the particle recycle among the various toroidal sectors during the beam injection. The effects of SMBI on the edge plasma temperature and density were detected by Langmuir probe array with 10 tips mounted on the graphite seat, which can be moved along the mid-plane and rotated 360° angle around the axis of the shaft.

Single channel HCN far infra-red interferometer was used to measure the central chord averaged electron density. A 2 mm microwave scanning heterodyne receiver (ECE) was used to measure the electron temperature profile under different discharge conditions.

3. Diagnostics in lower divertor of HL-2A

A special diagnostic instrument used for the HL-2A divertor neutralized plates, in which two arrays of Langmuir probes are installed on the inner- and outer-target plates respectively.[7] The inner and outer target plates are just vertical to the plasma mid-plane and both target radial location is $R = 139.95\,\mathrm{cm}$ and 163.35 cm respectively. Each probe array is composed of seven flush probes with 3 tips, which are located on the same toroidal section, as shown in Fig.1 and Fig.2. There are the spatial resolution of 1 cm in vertical direction and 1.5 cm in toroidal direction, the vertical positions of every probe on the outer target plate in the lower divertor chamber are listed in Fig.2. The position of the mid-plane of the main plasma is at $z = 0$.

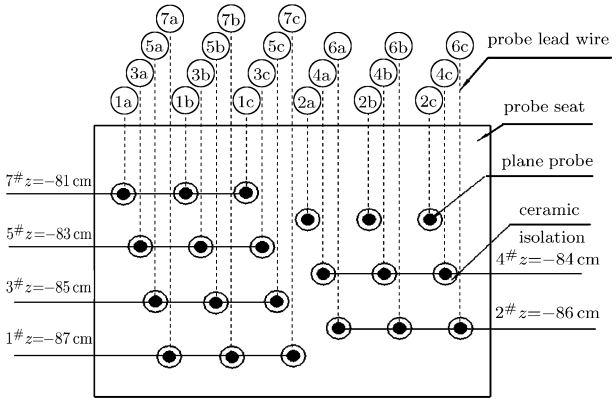


Fig.2. The arrangement of Langmuir probe array fixed on outer target plate in the HL-2A lower divertor.

A movable Langmuir probe was mounted in the outer divertor chamber to detect the radial distribution of electron temperature and density. The line-average electron density under both throats of the divertor chamber can be measured by 8 mm or 4 mm

microwave interferometer. Three channels optic fibres are applied to monitor visible emissions from the particles of working gas or impurities in the outer divertor. A home-made fast ionization gauge was used to measure the neutral gas pressure during the whole discharge period.

4. Experimental results of HL-2A divertor discharges

There are three field shaping coils (multi-pole field coils MP1, MP2 and MP3) in the lower divertor, the arrangement order of the coils from the strong field side to the weak field side is MP1, MP2 and MP3. According to the CF code simulation results for formation the divertor configuration, the current for MP2 coil is slightly higher than that for MP1 and MP3 in series.

4.1. Comparison between numerical simulation and experimental measurements

The well known CF code is adopted to quickly determine the shape and position of the plasma column, the location of X-point, the separatrix, and the magnetic flux in the SOL and the divertor region from the external magnetic measurements in HL-2A. The charged particles in the SOL area along the magnetic flux can pass through the inner and the outer toroidal throat into the lower divertor chamber, and strike on the inner and the outer target plates respectively. These striking points on inner plate and outer plate form two cylindrical striking zones. Figure 3 illustrates the special striking points, which pass through the X-points, versus time on the inner and outer target plate of lower divertor for shot 2896. In the mean while, the widths of striking zone on the inner and outer target plates and the widths of magnetic flux under the inner and outer throat at $z = -65\,\mathrm{cm}$ within lower divertor chamber versus time for shot 2896 are shown in Fig.4 respectively. The simulation results of the CF code illustrate that, the location and width of striking zone on inner and outer target plate is asymmetrical. The location and width of striking zone on the inner target plate are stable, the width is about 3.6 cm from $z = -79\,\mathrm{cm}$ to $-83\,\mathrm{cm}$ during $t = 240\,\mathrm{ms}$ to 800 ms, and the location of the special striking points versus time are constant. The widths of striking zone on outer target plate are unstable and the location of the special striking points versus time is variable. The unstable striking zone or the variable location of special striking point is resulted from the plasma column displacement.

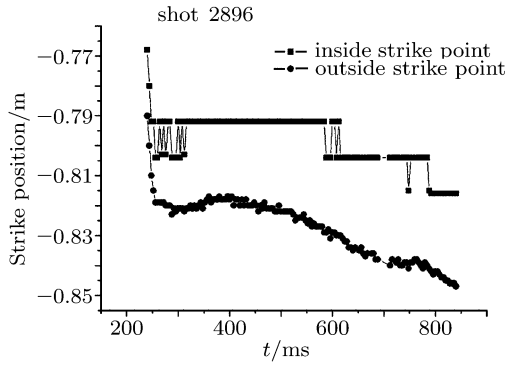


Fig.3. Positions of special striking point on the target plates versus time in lower divertor. The position of the main plasma mid-plane is on $z = 0$.

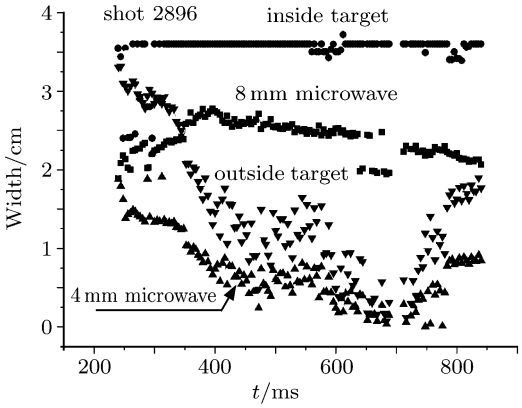


Fig.4. Widths of striking zone on the target plates and the widths of magnetic flux through the space between two microwave horns within lower divertor versus time. 8 mm microwave interferometer is located in inner divertor and 4 mm one is located in outer divertor.

The distributions of plasma electron density on the outer and the inner target plate for shot 2986 and their time evolution measured by Langmuir probe arrays are shown in Fig.5, and from the measured density distributions and their time evolution we can compare and check the location and widths of striking zone on the neutralizing plate simulated by the CF code. The measurable dimension with Langmuir probe array in z direction is about 7 cm on inner or outer target plate, and the measurement region can cover the whole striking zone in z direction. The real flux of plasma stream in the divertor is not uniform: for ex-

ample, in the inner target plate the signals of n_{ed9} and n_{ed12} is very small as shown in Fig.5. The magnetic flux in the SOL and the divertor region can simulated by the CF code but not the flux distribution, so the Langmuir probe array is a complementation for the CF simulation method. Fortunately, the simulation results obtained from CF code for the time and location evolution of the plasma stream striking zone on the target plates are in agreement with the measurement results by Langmuir probe array as compared between Fig.4 and Fig.5.

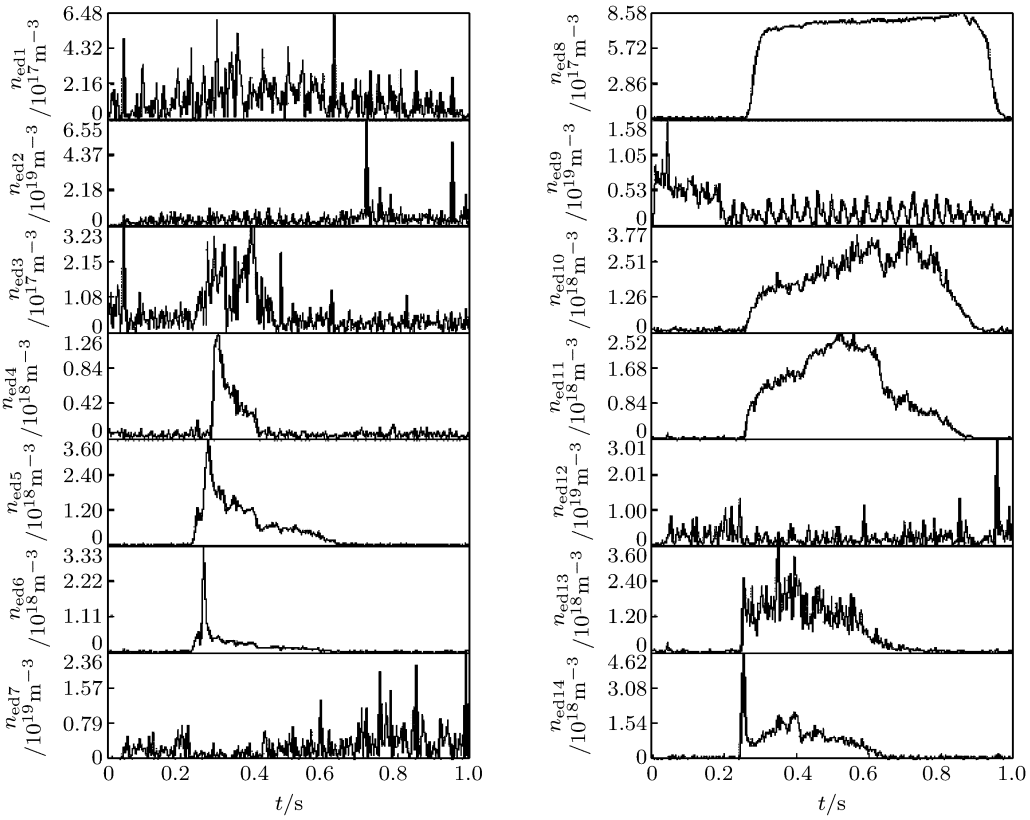


Fig.5. Electron density versus time on the outer target plate (N_{edd1-7}) and the inner target plate ($N_{edd8-14}$) in the lower divertor for shot 2896.

The distance between the two microwave horns is 12 cm, which is much longer than the width of the plasma across the microwave measurement line. The cross-section of the magnetic flux under both throats of the divertor chamber versus time can be accurately calculated with CF code, the width of the cross-section is 2.5 cm for the outer divertor chamber on $z = -65$ cm. The time evolution of density measured by the 8 mm microwave interferometer may compare with that measured by Langmuir probe array, and from the comparison of both measurement results we can check up the time evolutions of magnetic flux in the divertor obtained by the numerical simulation. Figure 6 shows that the line averaged electron density measured by the microwave interferometer is in good agreement with that measured by Langmuir probe array.

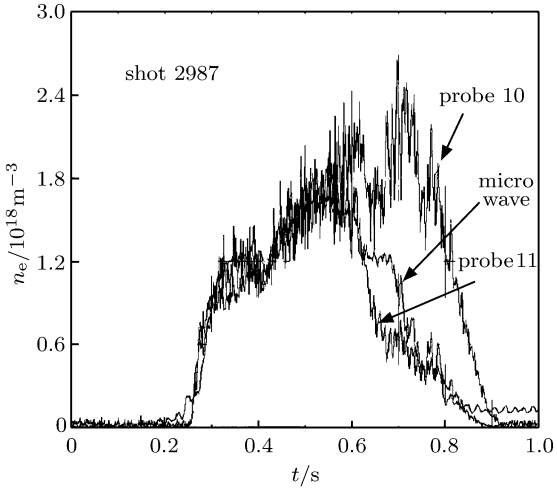


Fig.6. Comparison of electron density measured with Langmuir probe array (probe 10 and probe 11) on the inner target plate and with 8 mm microwave interferometer under the inner throat in the lower inner divertor.

So it is evident that the time evolution of density measured with the probe arrays in the lower divertor is reliable and the widths of striking zone on the neutralized plates are reasonable, which are simulated by CF code and checked by the Langmuir probe arrays.

4.2. Behaviour of SMBI into the HL-2A plasma

Ten hydrogen molecular beam pulses with low pressure 0.2 to 0.3 MPa, each pulse duration 10 ms and pulse period 30 ms, were injected at the mid-plane of the HL-2A torus along with the major radius from $t = 200$ ms and the divertor function was started up from the three field shaping coils (MP1, MP2, MP3) putting into operation at $t = 240$ ms. Before that time the HL-2A plasma was operated in the limiter configuration, the charged particles produced from the first two pulses of molecular beam can not appear in the divertor chamber. After $t = 240$ ms the fuelling particles from the later eight molecular beam pulses can enter into not only the main plasma, but also the divertor chamber. The variation of plasma electron density and temperature were detected by the HCN far infra-red interferometer and edge Langmuir probes in the main chamber, and by the Langmuir probe arrays and optical diagnostics in the lower divertor chamber, respectively. The fuelling characteristics of the SMBI into HL-2A plasma with and without lower closed divertor configuration for shot 2987 are shown in Fig.7.

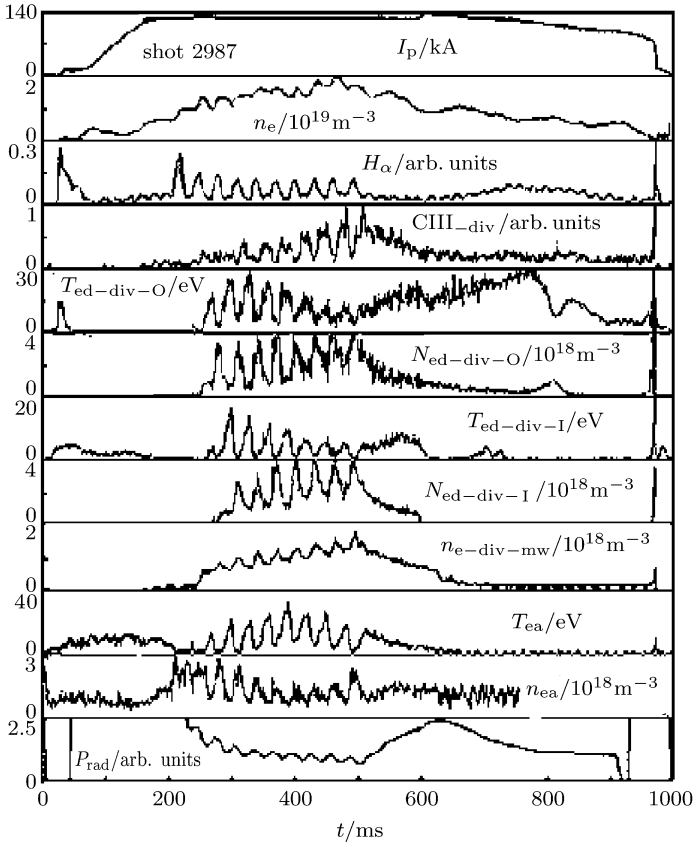


Fig.7. Behaviour of ten pulses of SMB injected into HL-2A plasma. Limiter configuration is before $t = 240$ ms and divertor one formation is after the time. I_p, n_e, H_α, n_{ea} and T_{ea} are plasma current, average electron density, H emission intensity from edge plasma on the low field side, electron density and electron temperature from edge plasma in the main chamber, respectively. $N_{ed-div-I}$, $N_{ed-div-O}$, $T_{ed-div-I}$ and $CIII_{-div}$ are electron density on inner plate, electron density on outer plate, electron temperature on inner plate and impurity of Carbon III emission intensity in the lower closed divertor chamber, respectively.

During the periods of SMB pulse injection the electron density nearby the neutralized plates of the divertor increases an order of magnitude than that in the intervals of the beam pulses under the situation of HL-2A divertor configuration. The plasma behaviour in the divertor chamber is dependent upon and in synchronism with that of the upstream plasma, especially the SOL plasma in the main plasma chamber. The electron density on the inner and outer target plate location $n_{\mathrm{ed-div-I}}$ and $n_{\mathrm{ed-div-O}}$ varies linearly with density n_{ea} in SOL, respectively, i.e. $n_{\mathrm{ed-div-I}} \cong n_{\mathrm{ed-div-O}} \cong 1.5 \times n_{\mathrm{ea}}$. On the other hand, the electron temperature on the target plate locations also varies linearly with the upstream temperature, $T_{\mathrm{ed-div-I}}$ is approximately equal to 2/3 of T_{ed} in SOL, as shown in Fig.7. During the period of SMBI fuelling, the electron temperature near by the target plate locations is less than 5 eV.

There is a boundary condition imposed on the conduction of heat in the SOL, which determines the power density q_{t} that can be convected through the electrostatic sheath at the target plate surface,[2]

$$q_{\mathrm{t}} = q_{\mathrm{k}} + q_{\mathrm{p}}, \tag{1}$$

where q_{k} is the kinetic power associated with the kinetic enthalpy of the flux of charged particles to the surface,

$$q_{\mathrm{k}} = n_{\mathrm{t}} c_{\mathrm{st}} \gamma T_{\mathrm{i}}, \tag{2}$$

where γ is the sheath heat transmission coefficient, approximately $\gamma = 7$, n_{t} and $c_{\mathrm{st}} = (2T_{\mathrm{i}}/m)^{1/2}$ are the density and ion acoustic speed at the target plate and m is the mass of an ion. T_{t} is the temperature at the target plate. q_{p} is the 'potential' power enthalpy which is convected through the sheath by the hydrogenic ions,

$$q_{\mathrm{p}} = n_{\mathrm{t}} c_{\mathrm{st}} \varepsilon_{\mathrm{pot}}, \tag{3}$$

where $\varepsilon_{\mathrm{pot}}$ is the potential energy per incident ion, this includes the ionization potential of a hydrogenic ion (13.6 eV) and half of the binding energy of a hydrogenic molecule (approximately 2.2 eV), thus $\varepsilon_{\mathrm{pot}} \approx 16$ eV, a constant.

The ratio of power density q'_{t}, during the SMBI period to q_{t}, before or after the beam injection, is as follows

$$\frac{q'_{\mathrm{t}}}{q_{\mathrm{t}}} = \frac{n'_{\mathrm{t}} c'_{\mathrm{st}} (\gamma T'_{\mathrm{t}} + \varepsilon_{\mathrm{pot}})}{n_{\mathrm{t}} c_{\mathrm{st}} (\gamma T_{\mathrm{t}} + \varepsilon_{\mathrm{pot}})}. \tag{4}$$

If $T_{\mathrm{i}} = T_{\mathrm{e}} = T_{\mathrm{t}}$ at the target plate, then

$$\frac{q'_{\mathrm{t}}}{q_{\mathrm{t}}} = \frac{n'_{\mathrm{e}}(7T'_{\mathrm{e}} + 16)}{n_{\mathrm{e}}(7T_{\mathrm{e}} + 16)} \sqrt{\frac{T'_{\mathrm{e}}}{T_{\mathrm{e}}}} = 0.4. \tag{5}$$

That is, during SMBI the heat load near by the target plate surface is just 0.4 times of that before or after the beam injection, which is very important for the divertor safety operation.

5. Conclusion and discussion

A series of SMB pulses were injected at the midplane of the HL-2A torus along with the major radius. The fuelling characteristics of the low pressure SMBI into HL-2A plasma with and without lower closed divertor configuration are evident. As analyses of the relationship for the electron density and temperature between the upstream and divertor regime, the HL-2A lower divertor was operated at the 'linear regime'. During the period of SMBI the temperature near by the target plate surfaces significantly decreases in the divertor. The heat load on the target plate surface is just 0.4 times of that before or after the beam injection. The first one of the objectives of divertor design is the wide dispersal of plasma power, which is most critical for a reactor, even in present machines. Therefore SMBI is a useful fuelling method for decreasing the heat load on the neutralized plates and to make a safe circumstance for the divertor operation.

Study on the lower single null divertor configuration of HL-2A tokamak was carried out with numerical simulation of CF code. The simulation results for the time and location evolution of the plasma stream striking zones on the target plates are in agreement with the measurement results by various diagnostics including the Langmuir probe arrays and the microwave interferometer in the lower divertor.

Acknowledgement

The authors wish to thank the HL-2A team members for their hard work.

References

[1] Liu Y, Ding X T, Yang Q W, Yan L W, Liu D Q, Xuan W M, Chen L Y, Song X M, Cao Z, Zhang J H, Cui C H, Cui Z Y, Deng Z C, Hong W Y, Hu H T, Huang Y, Kang Z H, Li B, Li W, Li F Z, Li G S, Li H J, Li Q, Li Y G, Li Z J, Liu Yi, Liu Z T, Luo C W, Mao X H, Pan Y D, Rao J, Shao K, Song X Y, Wang M, Wang M X, Wang Q M, Xiao Z G, Xie Y F, Yao L H, Yao L Y, Zheng Y J, Zhong G W, Zhou Y and Pan C H 2005 *Nucl. Fusion* **45** S239

[2] Pitchert C S and Stangeby P C 1997 *Plasma Phys. Control. Fusion* **39** 779

[3] Yuan B S, Liu L, You T X, Li F Z and Yang Q W 2004 *20th IAEA Fusion Energy Conference* (Nov. 1-6 2004 Vilamoura, Portugal) CN-116 / EX / pp5-35

[4] Jiao Y M, Zhou Y, Deng Z C, Ding X T, Liu Y and Wang E Y 2005 *Chin. Phys.* **14** 1600

[5] Yao L H, Dong J F, Zhou Y, Feng B B, Cao J Y, Li W, Feng Z, Zhang J Q, Hong W Y, Cui Z Y, Wang E Y and Liu Y 2004 *Nucl. Fusion* **44** 420

[6] Yao L H, Feng B B, Feng Z, Dong J F, Li W Z, Xu D M and Hong W Y 2002 *Acta Phys. Sin.* **51** 596 (in Chinese)

[7] Yan L W, Zhang J H, Yuan B S, Yan Q W, Li F Z and Hong W Y 2005 *Plasma Science & Technology* **7** 2797